Anthropomorphic Dual-Arm Coordinated Control for a Single-Port Surgical Robot Based on Dual-Step Optimization

Weibang Bai, Ziwei Wang, Qixin Cao*, *Member, IEEE,* Hiroshi Yokoi, *Member, IEEE,*
Masakatsu G. Fujie, *Fellow, IEEE,* Eric M. Yeatman, *Fellow, IEEE,* and Guang-Zhong Yang*, *Fellow, IEEE*

***Abstract*—Effective teleoperation of the small-scale and highly-integrated robots for single-port surgery (SPS) imposes unique control and human-robot interaction challenges. Traditional isometric teleoperation schemes mainly focus on end-to-end trajectory mapping, which is problematic when applied to SPS robotic control, especially for dual-arm coordinated operation. Inspired by the human arm configuration in boxing maneuvers, an optimized anthropomorphic coordinated control strategy based on a dual-step optimization approach is proposed. Theoretical derivation and solvability of the problem are addressed, and the effectiveness of the method is further demonstrated in detailed simulation and in-vitro experiments. The proposed control strategy has been shown to perform dexterous SPS bimanual manipulation more effectively, involving less instrument-interference and is free from singularities, thereby improving the safety and efficiency of SPS operations.**

***Index Terms*—SPS, Dual-step optimization, Anthropomorphic coordinated control strategy, Dual-arm configuration optimizing.**

I. Introduction

ROBOT assisted single-port surgery (SPS) and natural orifice transluminal endoscopic surgery (NOTES) are emerging trends in minimally invasive surgery (MIS). A single incision or patients' natural orifice is used to reach the surgical site, thus greatly reducing the access trauma. Recently, robot-assisted SPS operation has shown promises clinically as it simplifies control, improves precision and minimizes the surgeons involved. Other benefits include less pain, less blood loss, a lower risk of surgical complication and infection, and more rapid postoperative recovery [1]–[5].

There is thus far extensive research effort in developing miniaturized SPS robots. Issues related to mathematical modeling, kinematics analysis, system integration, and intelligent control algorithms are addressed and different hardware have also been proposed. For example, Webster et al. [6] and Dupont et al. [7] [8] proposed a type of continuum robots with pre-curved concentric tubes. Dario et al. [9] proposed the design and fabrication of SPRINT robot with on-board actuation mechanisms. Jeong et al. [10] developed a design for single port access laparoscopic surgery inspired by the structure of the elephant trunk. Simaan and Xu et al. [11]–[13] developed systems based on snake-like continuum robot arms actuated by NiTi tubes or stainless steel rods in push-pull configurations. Yang et al. proposed tendon driven platforms with different architectures including flexible arms made of superelastic Nitinol tubes with slots on the wall to enable two-directional flexibility, as well as flexible access i-Snake robot and single port Micro-IGES robot [14]–[18]. Shin and Kwon [19] proposed a surgical robot system for SPS, whose joint mechanism was based on wires and pulleys. Hong et al. [20] [21] designed the PLAS robotic system for SPS actuated using plate spring driven mechanisms with relatively high force transmission. Choi and Kim et al. [22]–[24] developed their SAIT robot system for SPS using variable neutral-line and wire-reduction mechanism embedded in instrument joint. Kobayashi and Fujie et al. [25] [26] proposed a novel robot system using linkage transmission based on double screw actuation mechanism driven by rotational flexible shafts.

In light of the conceptual principles and requirements of SPS operation, the existing SPS robots share common design features of multiple arms with high degree-of-freedoms (DOFs) equipped with surgical devices and endoscopes. Moreover, they also require miniaturized and highly integrated mechanical structure, high dexterity for tissue manipulation with sufficient triangulation and manoeuvrability in a small crowded in-vivo workspace, and controlled through teleoperation schemes. Nevertheless, the dense installation of miniaturised robotic arms and instruments may easily raise safety and efficiency issues, including self-interference and collision in the limited workspace, especially when performing coordinated manipulation [27], [28]. Besides being more compact with smaller size and higher dexterity, dual-arms are usually arranged for SPS robot with more constraints as they need to restore operational triangulation after parallelly going through the small incision [29]. Consequently, it is challenging to keep dual arms moving freely and safely without interference or instrument clashing within the confined workspace in terms of dexterous SPS.

However, safe and efficient coordinated control is essential for the clinical application of SPS robots. It needs to keep

W.Bai and Z.Wang contributed equally to this work. This work was supported by National Key R&D Program of China 2017YFC0110502, UK Wellcome Trust GB-CHC-210183, and UK EPSRC Programme Grant EP/P012779/1. *(Corresponding author: Qixin Cao, Guang-Zhong Yang.)*

Weibang Bai is with The Hamlyn Centre and the Department of Computing, Imperial College London, London, UK

Ziwei Wang is with the Department of Bioengineering, Imperial College London, London, UK

Qixin Cao is with the School of Mechanical Engineering, Shanghai Jiao Tong University, Shanghai, China (E-mail: qxcao@sjtu.edu.cn).

Hiroshi Yokoi is with Department of Mechanical Engineering and Intelligent Systems, The University of Electro-Communications, Tokyo, Japan.

Masakatsu G. Fujie is with the Healthcare Robotics Institute, Future Robotics Organization, Waseda University, Tokyo, Japan.

Eric M. Yeatman is with the Department of Electrical and Electronic Engineering, Imperial College London, London, UK

Guang-Zhong Yang is with the Institute of Medical Robotics, Shanghai Jiao Tong University, Shanghai, China (E-mail: gzyang@sjtu.edu.cn). He was with the Hamlyn Centre, Imperial College London, London, UK.

the highly integrated and closely distributed miniature arms cooperating with each other and avoiding collision or self-interference.

Although various actuation principles and mechanisms have been proposed to build SPS robots, most studies focused on basic kinematic modelling and teleoperation control design for the SPS robots. However, it is still challenging to satisfy the crucial demands on safety and coordinated control. Limited research has further studied on the common practical issue. For instance, Hong et al. tried to improve the noted safety issues of SPS robots in remote joint space by designing a special local device [21]. A novel coordinated control strategy for dual-arm teleoperation with a miniaturized robot for SPS was proposed in [27], while lacking the detailed analysis and methodological proof. Thus, the main contributions of this paper are as follows:

- The common issues of SPS robots and their fundamental causes are firstly addressed.
- A dual-step optimization approach is proposed to solve configuration optimization problems under multiple constraints.
- The theoretical derivation and proof of the anthropomorphic coordinated control strategy for the SPS robotic teleoperation are provided, which is formulated as the real-time optimization problem within both task space and joint space based on the proposed dual-step optimization approach.
- The effectiveness of the proposed method is validated with both analytical simulation and real experiments.

II. Problem Analysis

In general, robot-assisted SPS needs to solve the "chopsticks effect" [30] or leverage effect encountered when using traditional manually operation techniques. Nevertheless, the crowdedness of the miniaturized robotic instruments due to the close installation may cause safety and efficiency issues including self-interference or collision within a confined workspace, especially when completing coordinated manipulating tasks. To address the issue, we need to analyze the basic features and limitations of the robotic mechanism, the dual arm configuration, and the robotic teleoperation control.

A. Mechanism Constraints

The original concept of SPS robots was to simply integrate a few surgical instruments and allow them to pass through a single channel. The instruments may be curved and arranged parallelly or remain straight but crossed to reconstruct surgical triangulation inside the body. The general design consensus is that the ideal SPS robot for clinical applications should be with low external profile, low spatial occupation, multiple manipulator arms that are deployable through a single incision, and the capability of internal triangulation reconstruction [31].

Since miniature joints of the multiple arms are much closely distributed, instrument clashing of SPS robots occurs more easily when operating in narrow workspaces. The rate $\eta_d = \theta_d/\Omega \times 100\%$ indicating the drivable DOFs θ_d covered in the unit workspace Ω of the robot [27] can be adopted to

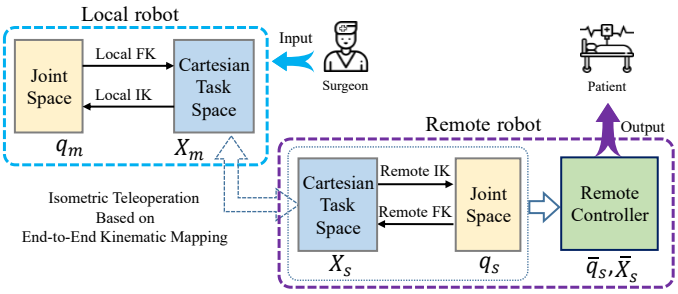

Fig. 1. Isometric teleoperation architecture.

analyze the common mechanism features. The higher the value of η_d, the more compact and more difficult it will be to control the multiple arms of the robot under the safety and efficiency constraints [27]. While, the rate η_d of SPS robot is much larger than that of traditional multiple key holes surgical robots and can be even in different scales in consideration of compact integration and relatively smaller workspace, which will have a significant impact on the safe and dexterous manipulation.

B. Limitation of Traditional Teleoperation

Teleoperation is usually adopted by surgical robot systems for MIS, where stability and transparency of the tele-control system are the main concerns [32]–[35]. Even though these elementary requirements are satisfied, traditional robotic teleoperation schemes are mainly developed based on end-to-end isometric kinematic mapping in task space as mechanical configurations on the local and the remote sides are always hard to keep the same. The teleoperation architecture relates joint space with the Cartesian task space through forward kinematics (FK) and inverse kinematics (IK). As shown in Fig.1, q_m and X_m represent the calculated joint state vector and pose vector of the local robot. q_s and X_s are the calculated remote robot joint vector and pose vector obtained from the mapping scheme. $\bar{q}_s$ and $\bar{X}_s$ are the real-time state of the remote robot joint and pose vector resulted updated by the remote controller.

The general kinematic algorithm is developed based on end-to-end mapping in task space on both sides. With the robotic FK and IK functions analytically described as $f_k(\cdot)$ and $f_k^{-1}(\cdot)$, and the pre-superscript m and s showing the local and remote side, the mapping function $g\left(q_m \mapsto q_s\right)$ can be expressed as $X_s = g(X_m) = g\left({}^m f_k\left(q_m\right)\right)$ and then target joint state of the remote robot arm is $q_s = {}^s f_k^{-1}\left(X_s\right) = {}^s f_k^{-1}\left(g\left({}^m f_k\left(q_m\right)\right)\right)$. The method can be implemented by combining basic motion scaling and configurational bias [36]–[38]. Consequently, with the homogeneous rotation and translation matrices, it can be expressed as:

$$\begin{bmatrix} R_s & P_s \\ 0 & 1 \end{bmatrix} = \begin{bmatrix} K_r R_m & K_p P_m \\ 0 & 1 \end{bmatrix} \oplus \begin{bmatrix} R_\zeta & P_\zeta \\ 0 & 1 \end{bmatrix} \quad (1)$$

where R and P with subscripts of m and s are rotation and translation parts for the local and remote side respectively, K_r and K_p are scaling factors, R_ζ and P_ζ are rotation and translation configuration bias values, and $\oplus$ represents the combination operator, one of which can be implemented by homogeneous matrix multiplication.

According to the kinematic mapping function, the traditional end-to-end strategy for teleoperation mainly focuses on pose

representation of the end target in task space, neglecting the remote robotic configuration in joint space. Neither the robot controller nor the local operator can recognize or predict potential configuration state hazards, thus it will be difficult to avoid these undesirable states for the remote robots when the joints or links are close to singularity, self-interference, collision, or other ill-conditioned states.

C. Solvability Foundation

Based on the above considerations, we can reformulate robot teleoperation mapping by adding joint configuration optimizing strategies in joint space beyond the basic trajectory tracking in task space.

Above all, the acceptable variance set of target poses lay the foundation of this solving method. For surgical robotic application, the following aspects would contribute to the variation of target pose: 1) Most of the surgical operating objects are soft, elastic or deformable, which allows certain degree of pose differences when operating [39], [40]. The visible and measurable variability would usually be in the order of millimeters. 2) Redundant orientation angles and tolerable flexible target positions for manipulation may exist because of task-based local kinematic redundancy and the robotic uncertainties like modelling and structural uncertainties. 3) Transmission backlash and assembly inconsistencies may cause inevitable structural uncertainties, and it can be exploited as possible extra motions passively generated when acting with external forces and thus providing objective tolerable poses.

As SPS robots are miniaturized and compact, the integration depends heavily on new types of structural design, power-driven and motion transmission schemes like continuum or discrete flexible mechanisms and tendon driven systems. As a result, uncertainties in kinematic and dynamic modelling and control are also unavoidable, hence the specific target pose of the robot end-effector can be located within a certain range. Therefore, we can define the resulted total range as a feasible neighborhood $S\left(X_d\right)$, which mainly incorporates the subsets caused by possible objective variability $S(P \mid \zeta)$, local task redundancy $S(P \mid \lambda)$, and robotic uncertainties $S(P \mid \delta)$. With the pose vector $X_d = \left[\begin{array}{cccccc} P_x & P_y & P_z & \varphi & \vartheta & \psi \end{array}\right]^T$, we have

$$S\left(X_d\right) = \left\{X_d \,|X_d \in S(P \mid \zeta) \cup S(P \mid \lambda) \cup S(P \mid \delta)\right\}. \tag{2}$$

In conclusion, SPS robots share common features in structural design and teleoperation control, thus having common safety and efficiency considerations. It is therefore necessary to propose robust solutions to improve the coordinated telemanipulating performance. The existence of the feasible neighborhood set resulted from structural uncertainty, local task redundancy, and possible objective variability provides the basis for developing a strategy to solve the above problems.

III. Dual-Step optimization Approach

Without loss of generality, to improve the states and performance of a given system, we can consider the following primal optimization problem (OP-I) for a class of electromechanical systems:

$$\text{OP-I}: \min_{q_i, \dot{q}_i} \quad \sum_{i=1}^{N} \alpha_i \left\|q_i - q_i^c\right\|^2 + \beta_i \left\|\dot{q}_i - \dot{q}_i^c\right\|^2$$
$$\text{subject to} \begin{cases} \alpha_i + \beta_i = 1, \\ f_k(q_i, \dot{q}_i) = 0, \quad k = 1, 2, \ldots, m \\ g_h(q_i, \dot{q}_i) \leq 0, \quad h = 1, 2, \ldots, n \\ q_{ij} \in [\underline{q}_{ij}, \bar{q}_{ij}],\ \dot{q}_{ij} \in [\underline{\dot{q}}_{ij}, \bar{\dot{q}}_{ij}] \end{cases} \tag{3}$$

where q_i and $\dot{q}_i$ are the ith system state and its differential subject to specific limitations. q_i^c and $\dot{q}_i^c$ are the reference state and their differential of q_i. $\alpha_i, \beta_i \in [0, 1]$ are the predefined weight coefficients. $f_k(q_i, \dot{q}_i)$ and $g_h(q_i, \dot{q}_i)$ stand for the kinematic and task-dependent differentiable convex constraints. The subscript j denotes the jth element of the corresponding variable. To facilitate later derivation, we combine state and task constraints as $g_h^*(q_i, \dot{q}_i) \leq 0, i = 1, 2, \ldots, n$. N is the degrees of freedom. Since the cost function in (3) is smooth and strictly convex, it is not necessary to construct the Lagrange dual function. Construct the Lagrangian function:

$$\begin{aligned} \mathcal{L}(q_i, \dot{q}_i, \lambda, \mu) = \sum_{i=1}^{N} \Bigg(& \alpha_i \left\|q_i - q_i^c\right\|^2 + \beta_i \left\|\dot{q}_i - \dot{q}_i^c\right\|^2 \\ & + \sum_{k=1}^{m} \lambda_k f_k(q_i, \dot{q}_i) + \sum_{h=1}^{n} \mu_h g_h^*(q_i, \dot{q}_i) \Bigg) \end{aligned} \tag{4}$$

where λ_k and μ_h are Lagrangian multipliers, which therefore lead to the Karush-Kuhn-Tucker (KKT) conditions:

$$\begin{cases} \nabla_{q_i} \mathcal{L} = 0, \nabla_{\dot{q}_i} \mathcal{L} = 0, & i = 1, 2, \ldots, N \\ f_k(q_i, \dot{q}_i) = 0, & k = 1, 2, \ldots, m \\ g_h^*(q_i, \dot{q}_i) \leq 0, & h = 1, 2, \ldots, n \\ \mu_h g_i^*(q_i, \dot{q}_i) = 0, & h = 1, 2, \ldots, n \\ \mu_h \geq 0, & h = 1, 2, \ldots, n \end{cases} \tag{5}$$

It implies the necessary conditions for the optimal solution of (3) are:

$$\begin{cases} 2\alpha_i(q_i - q_i^c) + \sum_{k=1}^{m} \lambda_k \frac{\partial}{\partial q_i} f_k(q_i, \dot{q}_i) \\ \qquad + \sum_{i=1}^{n} \mu_i \frac{\partial}{\partial q_i} g_i^*(q_i, \dot{q}_i) = 0, \\ 2\beta_i(\dot{q}_i - \dot{q}_i^c) + \sum_{k=1}^{m} \lambda_k \frac{\partial}{\partial \dot{q}_i} f_k(q_i, \dot{q}_i) \\ \qquad + \sum_{i=1}^{n} \mu_i \frac{\partial}{\partial \dot{q}_i} g_i^*(q_i, \dot{q}_i) = 0, \\ f_k(q_i, \dot{q}_i) = 0, \qquad k = 1, 2, \ldots, m \\ g_h^*(q_i, \dot{q}_i) \leq 0, \qquad h = 1, 2, \ldots, n \\ \mu_h g_h^*(q_i, \dot{q}_i) = 0, \quad i = 1, 2, \ldots, n \\ \mu_h \geq 0, \qquad i = 1, 2, \ldots, n \end{cases} \tag{6}$$

Since the constraints of (3) are convex, the saddle point of the Lagrange function (4) is the optimal solution to (3) by solving (6). It is worth pointing out that q_i^c and $\dot{q}_i^c$ are considered to be known in the process of solving the optimal problem (3). However, reference signals are often difficult to give artificially in advance, which need not only to satisfy the task and physical constraints, but also to achieve optimality under certain performance metrics. The reference signal therefore needs to be obtained by optimising. To this end, we consider the second primal minimization problem (OP-II) for

reference signals:

$$\begin{aligned} \text{OP-II}: \min_{q_i^c, \dot{q}_i^c} \quad & \mathcal{P} = \sum_{i=1}^{N} p(q_i^c, \dot{q}_i^c) \\ \text{subject to} \quad & \begin{cases} f_k(q_i^c, \dot{q}_i^c) = 0, k = 1, 2, \ldots, m \\ g_h^*(q_i^c, \dot{q}_i^c) \leq 0, h = 1, 2, \ldots, n \end{cases} \end{aligned} \tag{7}$$

where $p(q_i^c, \dot{q}_i^c)$ represents a performance metric that can be set according to actual task requirements and therefore need not be a convex function. Similarly with (4), we can obtain the Lagrangian function by introducing two variables u_k and ν_h ($\nu_h \geq 0$)

$$\begin{aligned} \mathcal{J}(q_i^c, \dot{q}_i^c, u, \nu) = \sum_{i=1}^{N} \Bigg(& p(q_i^c, \dot{q}_i^c) + \sum_{k=1}^{m} u_k f_k(q_i^c, \dot{q}_i^c) \\ & + \sum_{h=1}^{n} \nu_h g_h^*(q_i^c, \dot{q}_i^c) \Bigg). \end{aligned} \tag{8}$$

In this way, the Lagrange dual problem becomes:

$$\begin{aligned} \max_{u,\nu} \quad & \mathcal{H}(u, \nu) \\ \text{subject to} \quad & \nu_h \geq 0, h = 1, 2, \ldots, n \end{aligned} \tag{9}$$

which transforms (7) into a convex optimization problem. Here $\mathcal{H}(u, \nu)$ is the concave Lagrange dual function

$$\mathcal{H}(u, \nu) := \min_{q_i^c, \dot{q}_i^c} \mathcal{J}(q_i^c, \dot{q}_i^c, u, \nu) = \mathcal{J}(q_i^{c*}, \dot{q}_i^{c*}, u, \nu) \tag{10}$$

where $q_i^{c*}, \dot{q}_i^{c*}$ are the solution of $\nabla_{q_i^c} \mathcal{J}(q_i^c, \dot{q}_i^c, u, \nu) = 0, \nabla_{\dot{q}_i^c} \mathcal{J}(q_i^c, \dot{q}_i^c, u, \nu) = 0, i = 1, 2, \ldots, N$. Denote the primary and dual optimal values as $\mathcal{P}^*$ and $\mathcal{H}^*$, we have the weak duality property

$$\mathcal{P}^* \geq \mathcal{H}^*, \tag{11}$$

which indicates a nontrivial lower bound to approximate the optimal solution of (7). Thus, the problems OP-I and OP-II form the dual-step optimization approach to improve the specified performance of a system.

Remark 1. The robotic manipulability evaluation indices are important indicators normally used for evaluating the dexterity of the robot configuration, which exhibit significant nonlinearity and nonconvexity. After being transformed into a dual problem, the cost function is transformed into a linear one of single variable (ν), and the constraint condition is transformed into a simple convex constraint. Therefore, the process of solving the optimization problem (7) is simplified.

IV. Dual-Step Optimization Approach Based Anthropomorphic Coordination

In this section, a new real-time coordinated control strategy is proposed based on a defined anthropomorphic criterion derived from the customary resting state of human arms and the configuration of boxers' habitual preparing posture. By learning from human dual-arm movements, the possible solution of OP-II can be derived in (7). According to (11), the approximate optimal solution can be acceptable and the overall optimum is thus not necessary for the convenience of solving the problems.

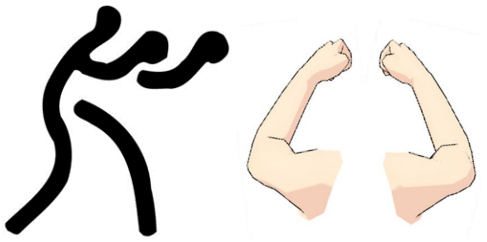

Fig. 2. Schematic configuration of boxers' preparation state.

A. Anthropomorphic Configuration Concept

It is intuitive that the similar boxing stance and arm configuration are mostly adopted when preparing an attack (see Fig. 2). The dual arms are kept in guard with the preparation pose with hands lifted and elbows down or bent outwards in opposite directions. Besides the defensive protection of the body, the preparation pose would avoid the dual arms moving with unsafe interference and collision, and secondly help to make the punching speed faster and the hitting motion more dexterous when attacking. Therefore, anthropomorphic control strategies inspired by the boxers' dual-arm postures can be derived to optimize the joint configuration, leading to improved triangulation and increased dexterity for SPS robots. The concept and theoretical derivations of the strategy were also submitted to the Ph.D. dissertation [41].

B. Anthropomorphic Criterion Configuration Definition

For further validation, indices that characterize the motion performance of the robot in different configuration can be adopted. Normally, we can choose indicators like condition number [42], manipulability [43], velocity manipulability ellipsoid [44], and directional manipulability (DM) [45] [46].

Detailed theoretical analysis and validation can be performed with our previous SPS robot system setup [28] [27], which was built with a hybrid serial-parallel structure based on discrete linkages connected double screw mechanisms and tendon rotational power transmission, and the kinematic models of the SPS robot and the parallel joint unit were presented in [27]. Here we can schematically abstract the kinematic chain of the major dual arms of the SPS robot, as shown in Fig.3.

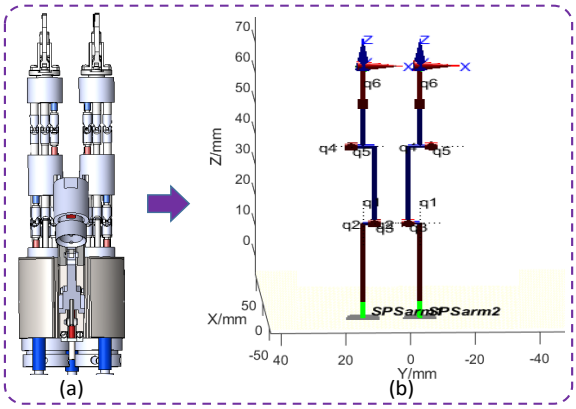

Fig. 3. Schematic kinematic chain abstraction of our SPS robot dual arms. (a) the 3D model of the SPS robot with dual operating arms and one endoscope supporting arm. (b) the abstraction kinematic chain of the dual operating arms and its visualization.

The manipulability ellipsoid enclosing the dexterous workspace indicates the ability of the robot to arbitrarily perform motion and change the position and orientation, which could measure the whole dexterity and manipulability of a given joint configuration. To indicate and compare the moving and manipulating performance of different joint configurations, we select three typical configurations of dual arms and visualize the distribution of their velocity manipulability ellipsoids, as demonstrated in Fig. 4. The unit sphere in the joint velocity space is defined as:

$$\dot{q}^T \dot{q} = 1. \tag{12}$$

Then the ellipsoid can be obtained by mapping it to the Cartesian space

$$v_e^T \left(J(q) J^T(q) \right)^{-1} v_e = 1. \tag{13}$$

where $J(q)$ and v_e are the Jacobian matrix and end-effector velocity. As shown in Fig. 4, three selected configurations of the dual arms, i.e., initial state, free state, and boxing state, are defined and analyzed accordingly. By comparing with different graphic visualization results, we can observe that the configuration of the boxing state Fig. 4(c), which is referred from the customary boxers' fighting preparation arm configuration is the best. This is because:

1) dual arms are both equipped with a much larger volume of the velocity manipulability ellipsoid, which means the whole dexterity and maneuverability are much better than other configurations;

2) more ellipsoid overlap between dual arms is obtained, which means they are sharing more free space for the dual arms' coordinated manipulating.

Consequently, we can conclude that according to the index of velocity manipulability ellipsoid, the defined optimizing criterion referred from the state of boxers' habitual preparing posture is much better in terms of maneuverability, dexterity and dual-arm operation. It is both intuitively and theoretically reasonable to identify and verify the intrinsic preponderance for coordinated control. Hence, this reference state can be used as the approximate solution of problem OP-II to further implement dual-arm configuration optimization for the SPS robot, although it may unnecessarily be the optimal state within its entire joint space, as constructed in (7) and (11).

C. Anthropomorphic Coordinated Control Strategy

Firstly, by adopting the traditional task space end-to-end mapping and trajectory following, a new control strategy with real time configuration optimization can be constructed. When received the local inputs and mapped into the remote target pose X_s for each arm, we can obtain the remote joint angle increment in the current control period

$$\dot{q}_s = J^{-1}(q) v_e^s = J^{-1}(q) \dot{X}_s. \tag{14}$$

The calculation $q_s = \int_{t_0}^{t} \dot{q}_s \, dt$ can be performed in discrete time, given the control interval Δt, the joint state at time t_k can be computed as:

$$q_s(t_k) = q_s(t_{k-1}) + \dot{q}_s(t_{k-1}) \Delta t. \tag{15}$$

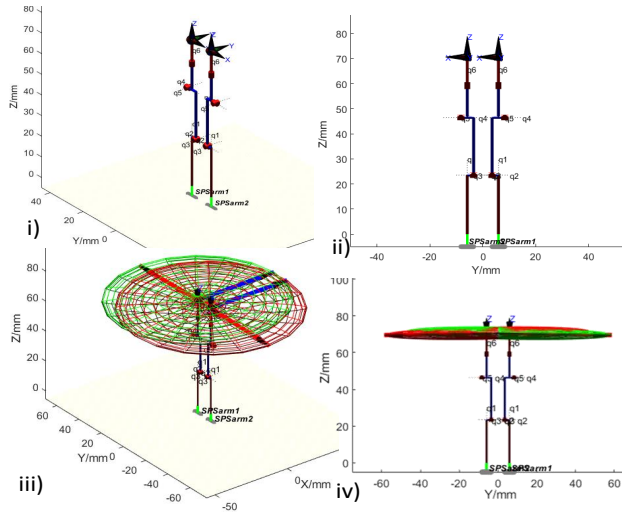

(a) Initial state: Dual arms keep straight.

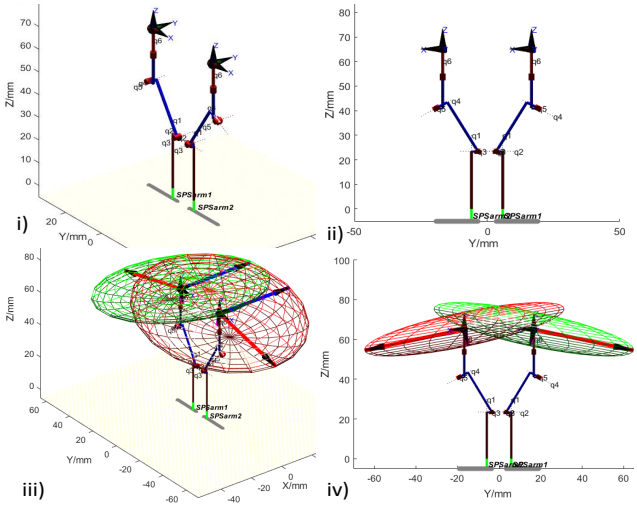

(b) Free state: Refer from human free or surrendering pose with hands up.

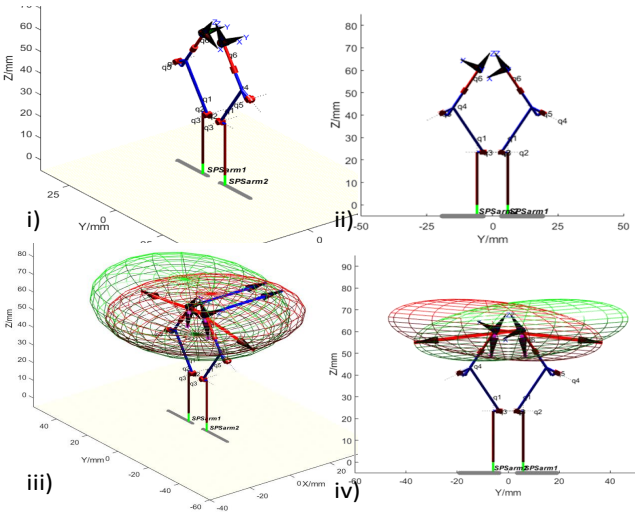

(c) Boxing state: Refer from customary boxing fight preparation arm shape.

Fig. 4. Typical anthropomorphic configurations definition and velocity manipulability ellipsoid visualization: In all three states (a), (b), and (c), i) and ii) show the side view and front view of the simplified dual arms' configuration respectively, iii) and iv) show the velocity manipulability ellipsoids distribution of the configuration with two views accordingly. Different colors and different views are used to clearly indicate the ellipsoids of the dual arms in every configuration.

By regarding the control interval as unit interval in high frequency robotic control loop, we can approximately use the numerical calculation:

$$q_s(t_k) \approx q_s(t_{k-1}) + \dot{q}_s(t_{k-1}). \tag{16}$$

However, before sending the calculated increment $\dot{q}_s$ directly to the remote robot's joint servo controller, we can build a strategy within the feasible configuration state set $S(q_d)$ and add an acceptable variation Δq_s replacing the value of $\dot{q}_s$ with $\dot{q}_s + \Delta q_s$, as shown in Fig.5, but keep the end target within the analyzed feasible neighborhood set $S(X_d)$ in task space. For the dual arms, the variation Δq_s can be defined with subscript L and R respectively:

$$\Delta q_s : \begin{cases} \Delta q_L = \left[\begin{array}{cccccc} \Delta q_{L1} & \Delta\vartheta_{L2} & \Delta\vartheta_{L3} & \Delta\vartheta_{L4} & \Delta\vartheta_{L5} & \Delta\vartheta_{L6} \end{array} \right]^T \\ \Delta q_R = \left[\begin{array}{cccccc} \Delta q_{R1} & \Delta\vartheta_{R2} & \Delta\vartheta_{R3} & \Delta\vartheta_{R4} & \Delta\vartheta_{R5} & \Delta\vartheta_{R6} \end{array} \right]^T \end{cases} \tag{17}$$

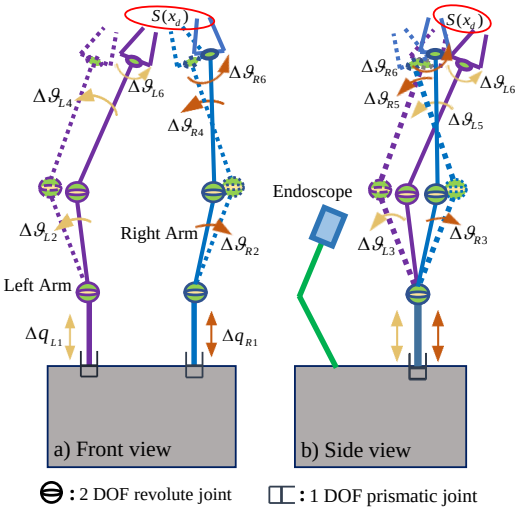

Fig. 5. Schematic diagram of the additional optimizing variation model based on the proposed strategy.

When specifying the feasible variation added in joint space, we can further adjust and improve the dual-arm configuration by calculating and choosing optimized variate Δq_{op} instead of just using the basic feasible Δq_s that meet the constraints, then the optimized joint increment can be updated and numerically calculated as:

$$\hat{\dot{q}}_s = \dot{q}_s + \Delta q_{op} \tag{18}$$

By changing the time period, the resulted joint state value should be:

$$\begin{gathered} \hat{q}_s(t+1) = q_s(t+1) + \hat{\dot{q}}_s(t), \\ \text{subject to} \quad \hat{q}_s, q_s \in S(q_d) \end{gathered} \tag{19}$$

Then we can construct the optimizing problem based on the demonstrated anthropomorphic coordinated method and design an objective function with constraints in both Cartesian task space and the joint space. The defined anthropomorphic criterion can be specified as Q^C_{arm}:

$$Q^C_{arm} : \begin{cases} {}^L Q_C = \left[\begin{array}{cccccc} {}^L q_{1C} & {}^L q_{2C} & {}^L q_{3C} & {}^L q_{4C} & {}^L q_{5C} & {}^L q_{6C} \end{array} \right]^T \\ {}^R Q_C = \left[\begin{array}{cccccc} {}^R q_{1C} & {}^R q_{2C} & {}^R q_{3C} & {}^R q_{4C} & {}^R q_{5C} & {}^R q_{6C} \end{array} \right]^T \end{cases} \tag{20}$$

In joint space, the optimizing control strategy can be built with an objective function aiming to make the dual-arm approaching the defined optimizing criterion configuration when building the teleoperation mapping:

$$S\langle q_s, X_s\rangle \leftarrow M\langle q_m, X_m\rangle \Rightarrow \min_{\hat{q}_s \in \mathcal{S}(q_d)} \left\| \hat{q}_s - Q^C_{arm} \right\|. \tag{21}$$

According to the constructed dual-step optimization approach, we can consequently define the OP-I as:

$$\begin{aligned} \arg\min_{\Delta X_d, \Delta q} \quad & \alpha \left\| \hat{q}_s(t+1) - Q^C_{arm} \right\| \\ \text{subject to} \quad & \begin{cases} q_s \in [q_{\min}, q_{\max}] \\ \hat{q}_s \in S(q_d) \\ |J(\hat{q}_s)| \neq 0 \\ v^s_e(t) = J_s(q_s(t))\, \dot{q}_s(t) \end{cases} \end{aligned} \tag{22}$$

where the singularity avoidance term $|J(\hat{q}_s)| \neq 0$ and joint limits of q_s are included.

But as addressed before, when adding configuration optimization by approaching the defined reference Q^C_{arm}, the end-effectors' poses will be changed and be different from the commanded target from the local side. Thus, we need to consider the acceptable pose error and make it be within the deduced feasible variation set $S(X_d)$ in the task space.

In Cartesian task space, the optimized control strategy can aim at the smallest difference or distance to a given target within the analyzed feasible neighborhood set when mapping:

$$S\langle q_s, X_s\rangle \leftarrow M\langle q_m, X_m\rangle \Rightarrow \min_{\Delta X_d \in S(X_d)} \left\| \Delta \hat{X}_d \right\|. \tag{23}$$

For this optimization objective, by using the similar construction method in joint space as (19) indicated, the chosen pose increment ΔX^{op}_s can be optimized within the basic feasible $\Delta \hat{X}_s$ that added the variation ΔX_d, and we have:

$$\begin{aligned} \Delta X^{op}_s(t+1) &= \min_{\Delta X_s \in S(X_d)} \left\| \Delta \hat{X}_s(t+1) \right\| \\ &= \min_{\Delta X_s \in S(X_d)} \left\| \hat{X}_s(t+1) - X_s(t) \right\| \\ &= \min_{\Delta X_s \in S(X_d)} \left\| X_s(t+1) + \Delta X_d(t) - X_s(t) \right\| \\ &= \min_{\Delta X_s \in S(X_d)} \left\| \Delta X_s(t) + \Delta X_d(t) \right\|. \end{aligned} \tag{24}$$

As the original $\Delta X_s(t)$ is given and determined by the local input and the mapping function, thus:

$$\min_{\Delta X_s \in S(X_d)} \left\| \Delta \hat{X}_s(t+1) \right\| \Leftrightarrow \min_{\Delta X_d \in S(X_d)} \left\| \Delta \hat{X}_d(t) \right\|. \tag{25}$$

So, to emphasize the consideration of task space accuracy term and minimise the resulted error as well, we can combine the two objectives in (21) and (23) together with constant coefficients α and β under the condition of $\alpha + \beta = 1$, and use the equivalence in (25), then the defined OP-I in (22) can be updated with an extra penalty term in task space. The added extra penalty term, which is essentially convertable to be defined in joint space by using the Jacobin matrix at current time and can be described as the inequality constraint of $g_h(q_i, \dot{q}_i) \leq 0,\ h = 1, 2, \ldots, n.$ in (3). Thus, it would not affect the solvability of the optimization problem, especially

when its weight is low or when using simplified empirical solving methods as defined later in this paper. Hence we have:

$$\begin{aligned}&\underset{\Delta X_d,\Delta q}{\arg\min}\ \alpha\left\|\hat{q}_s(t+1)-Q_{arm}^C\right\|+\beta\left\|\Delta\hat{X}_s(t+1)\right\|\\&\text{subject to}\begin{cases}q_s\in[q_{\min},q_{\max}]\\\hat{q}_s\in S\left(q_d\right)\\\Delta\hat{X}_s\in S\left(X_d\right)\\\left|J\left(\hat{q}_s\right)\right|\neq 0\\v_e^s(t)=J_s\left(q_s(t)\right)\dot{q}_s(t)\end{cases}\end{aligned}\tag{26}$$

However, before these to be implemented, the related variables need to be specified. The feasible set $S\left(X_d\right)$ can be divided into a sphere for positions with a radius of $\Delta\bar{X}_d^p$ and a cone for orientation angles with an apex angle of $\Delta\bar{X}_d^o$ around the given pose X_G, and it can be written as:

$$\begin{aligned}&S\left(X_d\right)=U\left(X_G,\Delta\bar{X}_d\right)\\&=\left\{X_d=\begin{bmatrix}X_d^p\\X_d^o\end{bmatrix},\Delta\bar{X}_d=\begin{bmatrix}\Delta\bar{X}_d^p\\\Delta\bar{X}_d^o\end{bmatrix}\middle|\begin{array}{l}\|X_G^p-x_d^p\|<\Delta\bar{X}_d^p\\\|X_G^o-x_d^o\|<\Delta\bar{X}_d^o\end{array}\right\}\end{aligned}\tag{27}$$

Before optimizing, the task space variate $\Delta X_d\in S\left(X_d\right)$ can be sampled within the feasible set with a common random function $\mathrm{rand}(a,b)$ that generates a a-by-b matrix with random elements uniformly distributed in $(0,1)$:

$$\Delta X_d:\left\{\Delta X_d\in S\left(X_d\right)\middle|\Delta X_d(t)=(2*\mathrm{rand}(a,b)-1)\cdot\frac{\Delta X_s(t)}{\|\Delta X_s(t)\|}\cdot\Delta\bar{X}_d\right\}\tag{28}$$

The joint space variate $\Delta q_s\in S\left(q_d\right)$ can be set as:

$$\Delta q_s(t)=K_\lambda\cdot\left(q_s(t)-Q_{arm}^C\right)\tag{29}$$

where

$$K_\lambda=\begin{bmatrix}f_1(\lambda)&&&\\&f_2(\lambda)&&\\&&\ddots&\\&&&f_n(\lambda)\end{bmatrix},\tag{30}$$

$$f_i(\lambda)=-\operatorname{sign}\left(q_i(t)-Q_i^C\right)\left\|q_i(t)-Q_i^C\right\|\Lambda_i,\tag{31}$$

and $\Lambda=\begin{bmatrix}\Lambda_1&\Lambda_2&\cdots&\Lambda_n\end{bmatrix}^T$, $\Lambda_i\in[0,1]$, $i=1,2,\cdots n$. n is the number of DOFs of the robot. During evaluation, the deviation coefficient Λ_i can be sampled and set as a random value for overall optimization, or by directly defining an empirical function according to the restrictions and principles of the optimizing concept:

$$\Lambda_i=\mathrm{rand}()\text{ or }f\left(\left|q_i(t)-Q_i^C\right|\right).\tag{32}$$

V. Simulation Results

To validate the proposed strategy and the further defined implementation, specific states of the defined variables can be assigned. The stated parameters are initialized in Table I. As indicated, the defined standard superior reference configuration Q_{arm}^C referred from the boxing state is unnecessarily to be optimal within the joint space, which shows the robustness and feasibility to implement. One can manually define and adjust it to make the dual-arms similar with the verified anthropomorphic standard state.

TABLE I
Variable Initialization

Variables	Definition	Values
Q_{arm}^C	${}^LQ_C$	$\begin{bmatrix}23.5&\frac{20\pi}{180}&0&-\frac{40\pi}{180}&0&0\end{bmatrix}^T$
	${}^RQ_C$	$\begin{bmatrix}23.5&\frac{20\pi}{180}&0&-\frac{40\pi}{180}&0&0\end{bmatrix}^T$
$\Delta\bar{X}_d$	$\Delta\bar{X}_d^P$	$3.5mm$
	$\Delta\bar{X}_d^O$	$\frac{6\pi}{150}rad$
$\mathrm{rand}(a,b)$	a	100
	b	1

Key parameters in the designed optimizing control strategy are initialized according to their analyzed and provided definition. Criterion configuration referred from the boxing preparation dual-arm state is assigned according to the SPS robot arm joint types and states, the unit for translation joint is mm, and rotation joint is degrees.

However, solving the resulted optimization problem (26) is complicated and computationally expensive although many methods and libraries can be used, because it is time varying, highly nonlinear, and multi-objective with multi-constraints. For real-time implementation, we can try to get a near optimal solution rather than the optimal one at each control interval, followed by adding suitable approximation variables for further optimization. Accordingly, the designed random variables and coefficients for iterative optimization can be implemented and initialized with requested properties that follow the target and the needed principles. And it can be empirically constructed as:

$$\begin{aligned}&\Lambda=f(x)=1-0.85^x\\&\text{subject to}\begin{cases}x=\left|q(t)-Q_{am}^c\right|\\\Lambda\leq[0.4\quad 0.2\quad 0.2\quad 0.3\quad 0.3\quad 0.2]^T\end{cases}\end{aligned}\tag{33}$$

Besides, by applying a simple combination, we can give the same weights to both objectives in the task and joint spaces, i.e. $\alpha=\beta=0.5$.

To validate the proposed coordinated control strategy, we can simulate a similar dual-arm cooperating surgical task by assuming we want to peel off the skin of a grape. The dual arms of the SPS robot start cooperating from a state close to the defined and assigned criterion configuration and trying to manipulate the target with and without applying the proposed anthropomorphic coordinated control strategy. The end trajectory of the dual arms firstly start from X_1, and draw close to the grape at the same time and reach X_2, and then both move outside like tearing the skin to X_3.

TABLE II
Simulation Task Trajectory Definition

Targets	Arms	State Values					
X_1	$L1$	0	-5.38	65.27	0	-0.35	-1.57
	$R1$	0	5.38	65.27	0	0.35	-1.57
X_2	$L1$	0	-2.5	64.5	0.1	-0.25	-1.12
	$R1$	0	2.5	64.5	-0.1	0.25	-1.12
X_3	$L1$	-2	-7.5	66.5	0.2	-0.15	-1.25
	$R1$	-2	7.5	66.5	0.2	0.15	-1.25

X represents the defined targets of 6 DOFs pose along the simulation task trajectory. For the dual arms system, L stands for Left arm, and R stands for Right arm. For the state values, the unit of position vector (first 3 columns) and orientation angle (last 3 columns) are mm and rad respectively.

The simulation trajectories of the coordinated manipulating task for dual arms are defined in Table II. When the proposed control strategy is applied, target trajectories will be changed. Then deviations or distance errors are generated, but they are still running within the defined feasible set for each target pose, which should be acceptable. The resulted trajectories of the simulation task with and without the proposed strategy, and the calculated trajectory error with the strategy are shown in Fig.6.

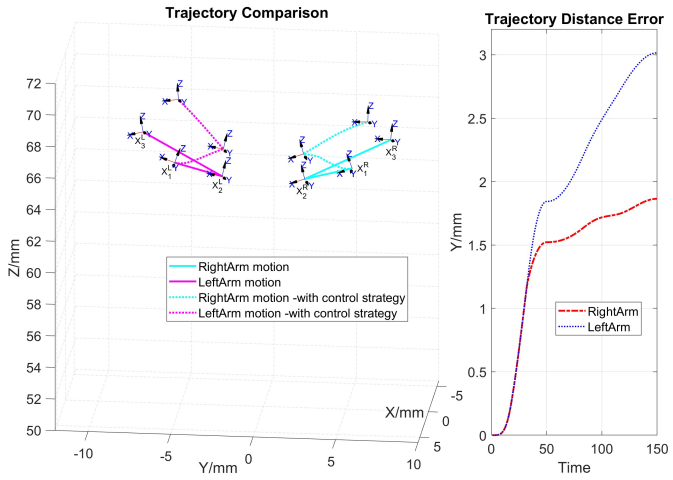

Fig. 6. Dual-arm task space trajectories comparison and the resulted trajectory deviations: The left figure shows the dual-arm trajectories of the simulation task, the defined motion without the strategy starts from X_1 to X_2 and reach X_3 for dual arms with superscripts L and R, while the dashed curves show the resulted motion with the proposed control strategy; the right figure shows the distance error of trajectories with deviation using the proposed strategy.

To quantitively evaluate the effect of the proposed coordinated control strategy, the index of task-based directional manipulability can be used. For the remote side SPS robot, we can define the pose change vector between the successive adjacent moments as the current task operational direction:

$$\mu(t) = X_s(t+1) - X_s(t) \tag{34}$$

Then the task-based directional manipulability along the operational direction can be calculated. For ease of comparison, natural logarithm processing of it can be further adopted:

$$DM'(t) = \log\left(\frac{1}{\mu(t)\left(J(t)J^T(t)\right)^{-1}\mu^T(t)}\right) \tag{35}$$

The joint states are also varied when using the proposed strategy for this simulated coordination task. As shown in Fig.7, compared to the solid lines with the original method, the dashed lines show the joint states are updated by the introduced variation according to the proposed strategy.

During the simulation procedures of the assumed coordinated manipulating task, the processed task-based DM of the dual arms are iteratively computed. As shown in Fig.8, red and blue curves respectively represent the results with and without the proposed strategy for dual arms. Take the time step 20 to 33 of the left arm motion for an example, the difference between them even reaches about 0.97, which means the enhanced DM is about $10^{0.97} \approx 9.3$ times of the one without adopting the proposed strategy. From the overall

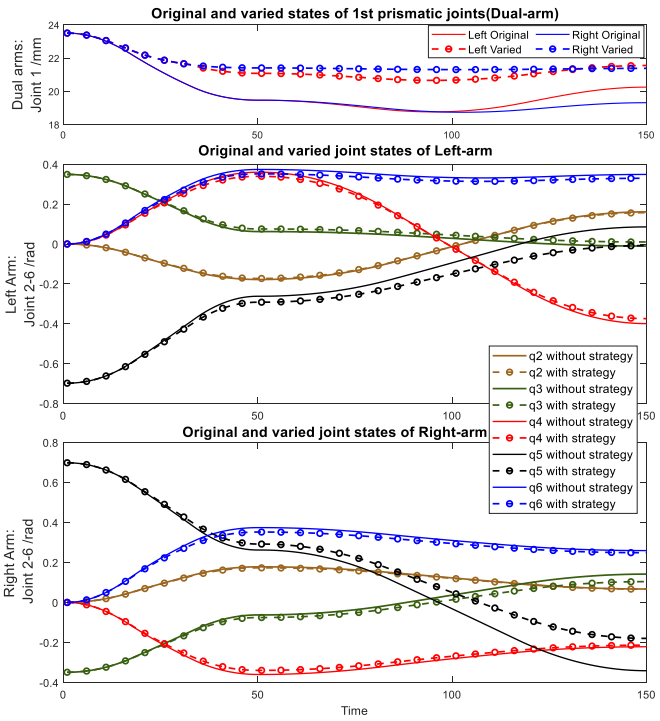

Fig. 7. Dual-arm joint states comparison between the original and the varied states: the solid lines show the original joint states and the dashed lines show the varied joint states after added the variation using the proposed strategy.

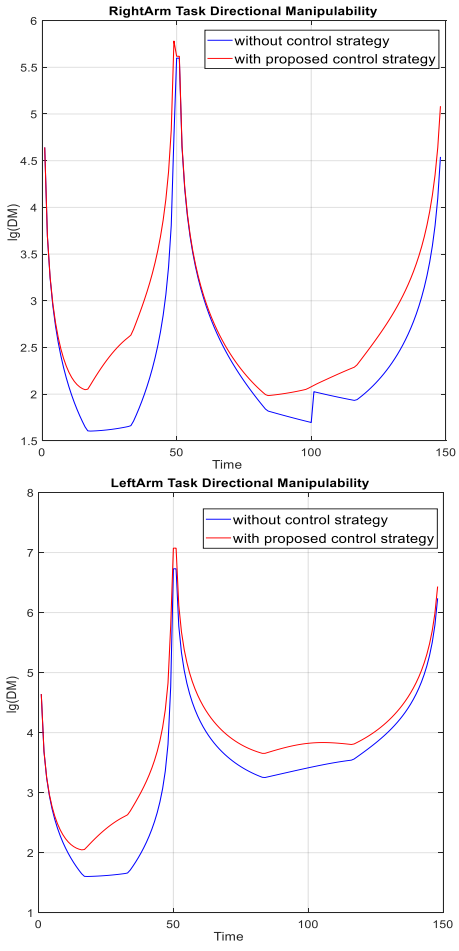

Fig. 8. Task directional manipulability of the dual arms during the simulation cooperating task with (red curve) and without (blue curve) proposed anthropomorphic coordinated optimizing control strategy.

comparison, it can be concluded that better manipulability during the whole operation process can be achieved when the proposed anthropomorphic coordinated control strategy is applied, even the optimization problem was solved with simplification and sub-optimal approximation by defining an empirical rule according to the desired concept.

Thus, its feasibility and effectiveness in improving the manipulability and dexterity of the SPS robot dual arms' coordinated manipulating can be verified. Moreover, with the obtained variation added to each joint using the defined empirical function and the additional restrictions for singularity and joint limit avoidance, the configurations during the motion are closer to the defined reference state, thus the safety problems of arm interference and singularities are avoided, and the ability to cooperatively manipulate within the confined surgical environment is enhanced.

VI. Experiments and Discussion

To further validate the proposed control strategy and examine the effect for coordinated surgical operation tasks, we completed different experiments including teleoperation in free-space, peeling off the skin of grapes, picking and cutting in-vitro animal tissues. And for the developed surgical robot system, in-vivo experiment was also designed to testify its basic application and to guide further research works.

A. Grape-skin Peeling-off Experiments

Beyond the simplified simulation task, the grape-skin peeling off experiments were basic and convenient, and we had completed it for more than 10 times. When peeling off the skin, the grapes were fixed with toothpicks on a plate of foam board from the bottom. To compare the tele-operating performance without and with the proposed coordinated control strategy, the statistical results were briefly recorded as shown in Table III. The main operating procedures with the proposed strategy are shown in Fig.9.

For this simple coordinated task, one arm kept still while the other arm moved outwards, which make it less risky of arm-interference, thus no additional strategy was deployed for them when operating without using the proposed strategy.

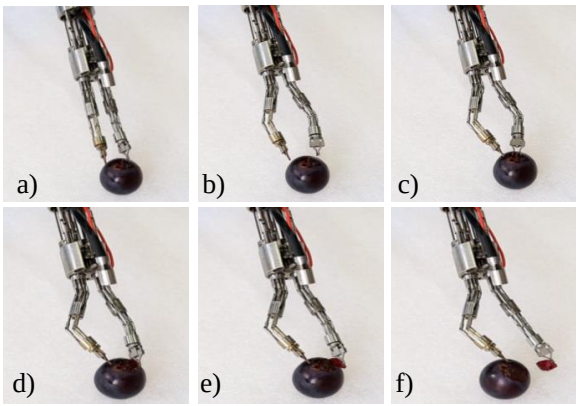

Fig. 9. Grape-skin peeling-off experiments with the proposed strategy: a) shows the initial state of the SPS robot, b) shows the preparation for the defined anthropomorphic criterion configuration, c) to e) shows the progress of holding the gripe by the right arm and peeling off the skin by the left arm, and the manipulating were improved with the proposed strategy, f) shows one piece of the skin was peeled off. The arms go back to the initial state of a) afterwards.

TABLE III
Comparison of Same Grape-skin Peeling Experiments With and Without the Proposed Coordinated Control Strategy

Coordinated control strategy	Number of tests	Task specifics		Motion safety	Mean operation time
		Grape mean size (ϕ)	Peeled skin area		
Without	6	$\approx 21.4mm$	1/4	Joint jerking happened 5 times	32s
With	6	$\approx 21.4mm$	1/4	Smooth and no jerking	25s

As indicated, for the same coordinated task, the dual-arm motion was safe and smooth with no arm collision when the proposed strategy was adopted, and the statistical mean operating time was 25s to peel-off a quarter of the surface area of the selected grapes, which was about 21% less. This demonstrated the valid improvement of safety and efficiency when completing this simple coordinating task using the proposed strategy.

B. In-vitro Experiments

The animal experiments were approved (No.20175001127) by the Animal Experimental Ethical Committee of Animal Experimental Center, Second Military Medical University in Shanghai. The previous tests [26] showed self-interference and collision between the highly integrated and closely distributed SPS dual arms could easily happen while tele-operating even without any target objects, and the experiments of peeling off the skin of grapes and operating on the porcine heart demonstrated the effectiveness of the proposed method.

The highly integrated SPS dual arms are closely distributed, with much higher rate η_d and other vigorous common features, thus collision avoidance for coordinated manipulating remains the fundamental safety issue. Without using the proposed anthropomorphic control strategy, the coordinated surgical task of cutting and picking up a piece of tissue was completed by using a normal cooperative scheme to avoid collision. This normal strategy was based on a real-time operating space reserving and rearrangement scheme, which always required one arm keep outside the core zone to make room for the other arm. The specific processes of this coordinated task are shown in Fig.10.

Another similar coordinated surgical task on an in-vitro porcine heart was selected but designed with more complexity and tougher demands. It was needed to move one arm to pick up the tissue, control the other arm equipped with electrocautery for cutting, and moved away the severed tissue thereafter.

In contrast, this more demanding coordinated surgical task was completed using the proposed anthropomorphic coordinated control strategy and its simplified solution. After initialized to be parallelly straight, the SPS robot dual arms started from a configuration near to the criterion defined and referred from the boxing preparation state, and manipulated the tissues with real time approaching the criterion to achieve configuration optimizing in each tele-control period, and also to make

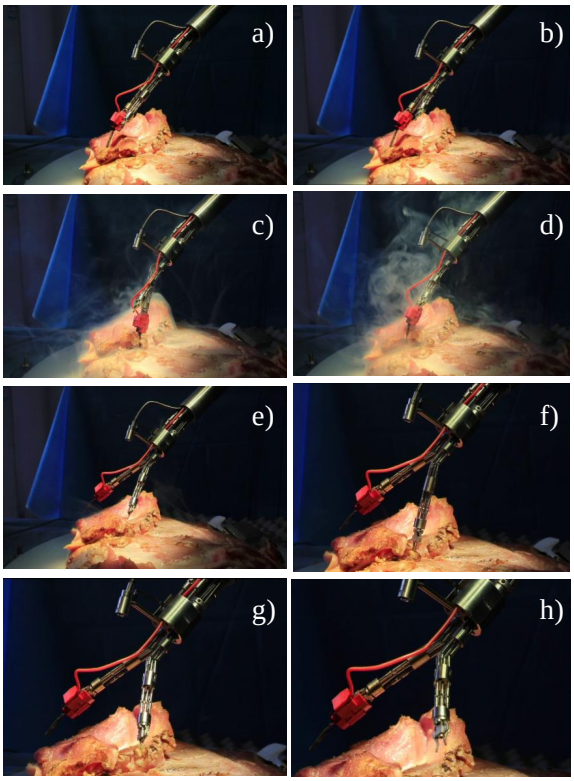

Fig. 10. In vitro experiment of dual-arm coordinated task with normal strategy: from a) to h) shows the progress of cutting tissue with the right arm equipped with electrocautery, picking up the chopped tissue to move and put down with the left arm. The collision avoidance scheme was based on normal strategy of operating space reserving and rearrangement.

it operate with better manipulability and less possibility of interference and singularity. The highly integrated and closely distributed dual arms with vigorous common features and common telecontrol problems were teleoperated cooperatively and dexterously at the same time. The specific procedures were recorded as shown in Fig.11. Results indicated no safety problems of interference, collision, and singularity occurred.

For further validation, the comparison analyses of the two in-vitro tasks are shown in Table IV. As indicated, the efficiency of the teleoperation with the normal strategy and the proposed anthropomorphic coordinated control strategy are obviously different. When using the proposed strategy, it took nearly 30% less operation time although performing a similar but more complex task, which demonstrated the effectiveness of the method.

TABLE IV
COMPARISON OF IN-VITRO EXPERIMENTS WITH DIFFERENT DUAL-ARM COORDINATED MANIPULATING STRATEGIES

Control strategy modes	Dual-arm coordinated tasks	Task difficulty	Efficiency	Safety	
			Operation time	Singularity	Interference
Normal strategy	Tissue cutting and moving ×	Easy	45s	Occasionally (Manually Guaranteed)	Occasionally (Manually Guaranteed)
Proposed strategy	Auricle tissue picking up and cutting +	Hard	32s	Optimized and avoided	Improved and not happened

×: Tissue dissection with one arm, pick up and put down with another, shown in Fig.10. +: Pick up the auricle with one arm and move the isolated tissue away after cutting by another arm, shown in Fig.11. The interference times during the operation was affected by the operational experience, movement speed, and continuous caution of the tele-operator. It was manually guaranteed by terminating before being too dangerous during the experiments.

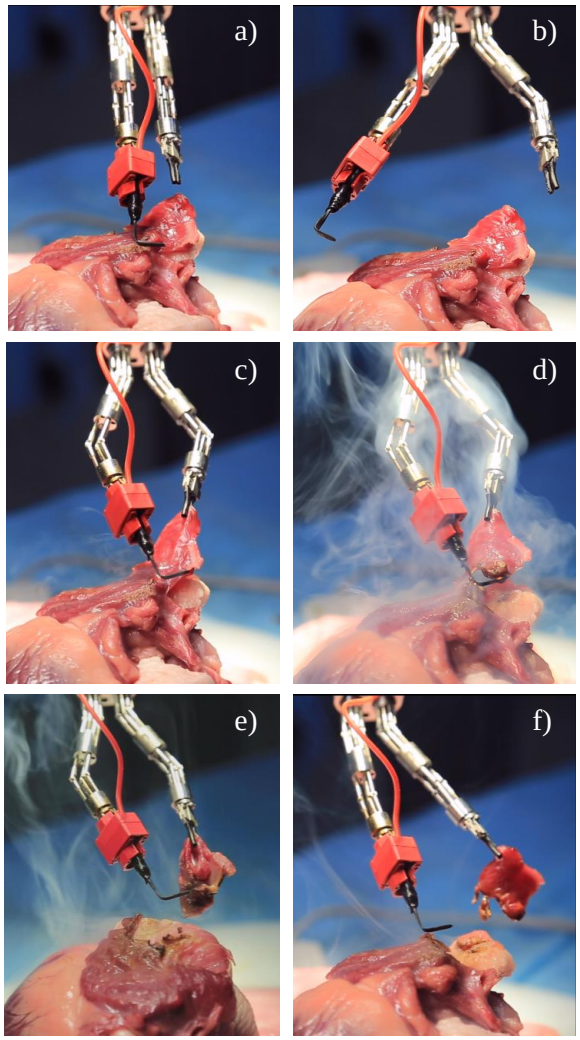

Fig. 11. In vitro experiment of dual-arm coordinated task with the proposed coordinated control strategy for porcine auricle cutting: a) the initialized parallel state; b) trying to reach the derived and defined criterion reference configuration; c) to e) picking up the auricle with one arm and cutting tissue with the other arm equipped with electrocautery, and the cooperating procedures were completing at the same time with the proposed optimizing control strategy using its defined simplified solutions; and f) move out the chopped tissue.

C. Discussion

The simulation example testified the theoretical analyses and derivations of the proposed coordinated control strategy, and the simplified solution constructed for solving the problem. In contrast, the grape-skin peeling experiments and in-vitro experiments on our SPS robot confirmed the effectiveness of the proposed strategy in improving the SPS robot for coordinated tele-manipulating with typical surgical tasks. The noted coordinating safety risks of self-interference or collision, and singularity of the miniaturized but highly integrated multiple arms were reduced, and higher tele-operating efficiency with less operating time was achieved.

During implementation and validation of the proposed strategy, we have simplified a few steps to make it feasible and applicable in the teleoperation control. Firstly, a referential but proven superior configuration, inspired by boxers' state of preparation, is directly adopted as an approximate solution to the optimization problem OP-II. The obtained anthropomor-

phic criterion is then used to construct the optimization problem OP-I for the dual arms. To further improve the SPS robot's dual-arm coordination performance, by adopting the dual-step optimization based approach, the overall optimal state (i.e. the optimum solution of OP-II) for the dual-arm coordination tasks can be further analyzed and adopted. Secondly, for the core variables defined in the algorithms like the feasible neighborhood set $S(X_d)$ and the superior criterion reference configuration Q^C_{arm}, the initial assignment can be arranged and adjusted specifically according to different surgical tasks and corresponding anatomical constraints. Thirdly, for solving the derived complex optimization problem, the compromised and simplified approach of defining an empirical function method is adopted. Thereupon, more solvers and libraries with good real-time performance and convergence properties can be further deployed, then the overall optimal solution and thus better improvement of the coordinated tele-control for the highly integrated SPS robot can be achieved. Fourthly, the combination weights of the two objectives in both task and joint spaces can be further analyzed and used to enhance the proposed strategy.

For the evaluation of the experiments presented above, the current quantitative analysis is still inadequate due to the difficulty in mounting sensors onside the miniaturized and compact manipulators for data collection and the risk of doing experiments with the fragile and unstable structures. The basic information of coordinated task efficiency was mainly indicated by mean operation time. In terms of coordination safety, the rough indices like joint jerking times for smooth motion and interference situation for coordination performance were mainly used. The better quantitative evaluation can be obtained with more mature tests on different robot platforms.

Furthermore, the proposed strategy could be further suitable with other SPS robots as this new type of surgical robots is sharing the same core design and integration features and suffering from the common coordinated control problems. Thus, the proposed concept and strategy could be the possible reference for solving the common problems of SPS robot dual-arm tele-manipulating.

In addition, after obtaining the permission from the Animal Experimental Ethical Committee, we also attempted to complete in-vivo experiments on an anesthetized pig. The selected target was to cut a designated tumor on the parenteral epidermis, and the SPS robot was teleoperated to complete the appointed task under professional instructions of veterinarians. The basic task was carried out, but unfortunately the test of the proposed strategy was not completed due to the inadequate surgical inner space caused by the air impermeability failure of the system. To present our investigation and insight about the integrity and consistency of research on surgical robot systems aiming to clinical applications, we provide this effort here and the procedures are shown in Fig.12.

After the in-vivo experiment, we found that more clinical application concerns including the working modes of surgical trocar, air impermeability around the incision, endoscopic view adjusting, depth information, inflation and workspace maintenance etc. are needed to be addressed. The designed in-vivo surgical task examined the schematic integration of the SPS robot system, the control system, and different control schemes and methods. But further investigation and exploration about core surgical concerns, advanced robotic techniques, and intelligent operating strategies like the proposed coordinated control strategy are highly needed, which would make surgical robots more applicable and effective.

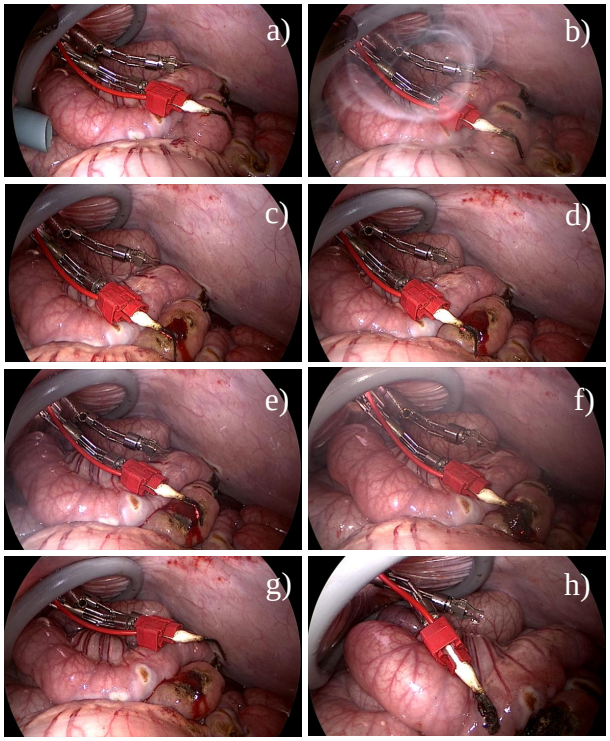

Fig. 12. In-vivo experiment of SPS robot system: a) go inside operative region after anesthesia and create a proper incision and try to find the target with the help of veterinarian; b) to c) try cutting and scraping the designated tumour on the parenteral epidermis with electrotome; d) the operated intestine was bleeding; e) to f) trying hemostasis with electrocoagulation; g) to h) finish and check again the task and prepare to retrieve.

VII. Conclusion

In summary, we analyzed the common problems caused by structural and control features of SPS robots, and especially addressed the safety and efficiency problems of the highly integrated and closely distributed dual arms of the SPS robot when tele-manipulating for coordinated surgical tasks. Thus, a novel anthropomorphic coordinated control strategy based on a proposed dual-step optimization approach was proposed and developed to solve the problem.

Inspired by the normally ease states of human dual-arm behaviors and the widely adopted boxing preparing configuration, a superior anthropomorphic criterion configuration for dual-arm coordinated maneuver was intuitively defined and theoretically proven. The obtained criterion reference was directly adopted as the approximate solution for the defined OP-II, and then used in OP-I. The proposed coordinated control strategy was thus constructed based on real-time optimization and approaching the defined criterion reference configuration in the remote joint space.

For further analysis and validation, the existence and solvability of the problems were addressed. The concept definition and theoretical proof and derivation were introduced.

With the theoretical evaluation based on the chosen robotic performance indices, the referenced boxing preparation state is intuitively, theoretically, and experimentally shown to be superior in terms of better manipulability and feasibility for dual-arm coordinated manipulation, although may not be the overall optimal state, as indicated when solving the OP-II. The derived anthropomorphic coordinated control strategy thus is reasonable to build the optimizing criterion configuration for the remote robot dual arms when teleoperating. Finally, the in-vitro experiments were completed, and the comparison results demonstrated the feasibility, effectiveness, and superiority for the demanding coordinated surgical tasks. Beyond the developed remote joint configuration optimizing concept and method, joint configuration perception and prediction strategies can also be further investigated in the future work.

ACKNOWLEDGMENT

The main work had been submitted as the Ph.D. dissertation to Shanghai Jiao Tong University, and has not been published anywhere else. The authors would thank the great help from the animal experiment center in Shanghai.

REFERENCES

[1] D. Samarasekera and J. H. Kaouk, "Robotic single port surgery: Current status and future considerations," *Indian J. Uro.*, vol. 30, no. 3, p. 326, 2014.

[2] J. H. Kaouk, R. J. Stein, and G.-P. Haber, *Atlas of Laparoscopic and Robotic Single Site Surgery*. Humana Press, 2017.

[3] J. Troccaz, G. Dagnino, and G.-Z. Yang, "Frontiers of medical robotics: from concept to systems to clinical translation," *Annu. Rev. Biomed. Eng.*, vol. 21, pp. 193–218, 2019.

[4] W. Bai, Q. Cao, P. Wang, P. Chen, C. Leng, and T. Pan, "Modular design of a teleoperated robotic control system for laparoscopic minimally invasive surgery based on ros and rt-middleware," *Ind. Robot*, vol. 44, no. 5, pp. 596–608, 2017.

[5] B. Chen, Q. Cao, and W. Bai, "A design of surgical robotic system based on 6-dof parallel mechanism," in *Int. Conf. Biolog. Inform. Biomed. Eng. (BIBE)*. VDE, 2018, pp. 1–5.

[6] R. J. Webster III, J. M. Romano, and N. J. Cowan, "Mechanics of precurved-tube continuum robots," *IEEE Trans. Robot.*, vol. 25, no. 1, pp. 67–78, 2008.

[7] J. Lock, G. Laing, M. Mahvash, and P. E. Dupont, "Quasistatic modeling of concentric tube robots with external loads," in *Proc. IEEE/RSJ Int. Conf. Intell. Robots Syst. (IROS)*. IEEE, 2010, pp. 2325–2332.

[8] J. Ha, F. C. Park, and P. E. Dupont, "Elastic stability of concentric tube robots subject to external loads," *IEEE Trans. Biomed. Eng.*, vol. 63, no. 6, pp. 1116–1128, 2015.

[9] M. Piccigallo, U. Scarfogliero, C. Quaglia, G. Petroni, P. Valdastri, A. Menciassi, and P. Dario, "Design of a novel bimanual robotic system for single-port laparoscopy," *IEEE/ASME Trans. Mechatron.*, vol. 15, no. 6, pp. 871–878, 2010.

[10] H. Jeong, J. Cheong, and S. Lee, "Multi-jointed integrated medical instrument system for single port access laparoscopic surgery," in *ICCAS 2010*. IEEE, 2010, pp. 134–138.

[11] K. Xu, R. E. Goldman, J. Ding, P. K. Allen, D. L. Fowler, and N. Simaan, "System design of an insertable robotic effector platform for single port access (spa) surgery," in *Proc. IEEE/RSJ Int. Conf. Intell. Robots Syst. (IROS)*. IEEE, 2009, pp. 5546–5552.

[12] N. Simaan, K. Xu, W. Wei, A. Kapoor, P. Kazanzides, R. Taylor, and P. Flint, "Design and integration of a telerobotic system for minimally invasive surgery of the throat," *Int. J. Robot. Res.*, vol. 28, no. 9, pp. 1134–1153, 2009.

[13] K. Xu, J. Zhao, and M. Fu, "Development of the sjtu unfoldable robotic system (surs) for single port laparoscopy," *IEEE/ASME Trans. Mechatron.*, vol. 20, no. 5, pp. 2133–2145, 2014.

[14] J. Shang, C. J. Payne, J. Clark, D. P. Noonan, K.-W. Kwok, A. Darzi, and G.-Z. Yang, "Design of a multitasking robotic platform with flexible arms and articulated head for minimally invasive surgery," in *Proc. IEEE/RSJ Int. Conf. Intell. Robots Syst. (IROS)*. IEEE, 2012, pp. 1988–1993.

[15] J. Shang, D. P. Noonan, C. Payne, J. Clark, M. H. Sodergren, A. Darzi, and G.-Z. Yang, "An articulated universal joint based flexible access robot for minimally invasive surgery," in *Proc. IEEE Int. Conf. Robot. Autom. (ICRA)*. IEEE, 2011, pp. 1147–1152.

[16] J. Shang, K. Leibrandt, P. Giataganas, V. Vitiello, C. A. Seneci, P. Wisanuvej, J. Liu, G. Gras, J. Clark, A. Darzi *et al.*, "A single-port robotic system for transanal microsurgery—design and validation," *IEEE Robot. Autom. Lett.*, vol. 2, no. 3, pp. 1510–1517, 2017.

[17] K. Leibrandt, P. Wisanuvej, G. Gras, J. Shang, C. A. Seneci, P. Giataganas, V. Vitiello, A. Darzi, and G.-Z. Yang, "Effective manipulation in confined spaces of highly articulated robotic instruments for single access surgery," *IEEE Robot. Autom. Lett.*, vol. 2, no. 3, pp. 1704–1711, 2017.

[18] P. Wisanuvej, G. Gras, K. Leibrandt, P. Giataganas, C. A. Seneci, J. Liu, and G.-Z. Yang, "Master manipulator designed for highly articulated robotic instruments in single access surgery," in *Proc. IEEE/RSJ Int. Conf. Intell. Robots Syst. (IROS)*. IEEE, 2017, pp. 209–214.

[19] W.-H. Shin and D.-S. Kwon, "Surgical robot system for single-port surgery with novel joint mechanism," *IEEE Trans. Biomed. Eng.*, vol. 60, no. 4, pp. 937–944, 2013.

[20] B. Cheon, E. Gezgin, D. K. Ji, M. Tomikawa, M. Hashizume, H.-J. Kim, and J. Hong, "A single port laparoscopic surgery robot with high force transmission and a large workspace," *Surg. Endosc.*, vol. 28, no. 9, pp. 2719–2729, 2014.

[21] S. Shim, T. Kang, D. Ji, H. Choi, S. Joung, and J. Hong, "An all-joint-control master device for single-port laparoscopic surgery robots," *Int. J. Comput. Ass. Rad. Surg.*, vol. 11, no. 8, pp. 1547–1557, 2016.

[22] J. Lee, Y.-J. Kim, S.-g. Roh, J. Kim, Y. Lee, J. Kim, B. Choi, and K. Roh, "Tension propagation analysis of novel robotized surgical platform for transumbilical single-port access surgery," in *Proc. IEEE/RSJ Int. Conf. Intell. Robots Syst. (IROS)*. IEEE, 2013, pp. 3083–3089.

[23] Y.-J. Kim, S. Cheng, S. Kim, and K. Iagnemma, "A stiffness-adjustable hyperredundant manipulator using a variable neutral-line mechanism for minimally invasive surgery," *IEEE Trans. Robot.*, vol. 30, no. 2, pp. 382–395, 2013.

[24] J. Lee, J. Kim, K.-K. Lee, S. Hyung, Y.-J. Kim, W. Kwon, K. Roh, and J.-Y. Choi, "Modeling and control of robotic surgical platform for single-port access surgery," in *Proc. IEEE/RSJ Int. Conf. Intell. Robots Syst. (IROS)*. IEEE, 2014, pp. 3489–3495.

[25] Q. Liu, Y. Kobayashi, B. Zhang, J. Ye, E. Inko, Y. Cao, Y. Sekiguchi, Q. Cao, M. Hashizume, and M. G. Fujie, "Design of an insertable surgical robot with multi-level endoscopic control for single port access surgery," in *Proc. IEEE Int. Conf. Robot. Biomimetics (ROBIO)*. IEEE, 2013, pp. 750–755.

[26] Y. Kobayashi, Y. Sekiguchi, T. Noguchi, Y. Takahashi, Q. Liu, S. Oguri, K. Toyoda, M. Uemura, S. Ieiri, M. Tomikawa *et al.*, "Development of a robotic system with six-degrees-of-freedom robotic tool manipulators for single-port surgery," *Int. J. Med. Robot.Comput. Assist. Surg.*, vol. 11, no. 2, pp. 235–246, 2015.

[27] W. Bai, Q. Cao, C. Leng, Y. Cao, M. G. Fujie, and T. Pan, "A novel optimal coordinated control strategy for the updated robot system for single port surgery," *Int. J. Med. Robot. Comput. Assist. Surg.*, vol. 13, no. 3, p. e1844, 2017.

[28] W. Bai, Y. Cao, P. Wang, Y. Kobayashi, M. G. Fujie, and Q. Cao, "Development of a new control system for the robotic single port surgery," in *Proc. 11th Asia. Conf. Comput. Aided Surg. (ACCAS)*.

[29] V. Vitiello, S.-L. Lee, T. P. Cundy, and G.-Z. Yang, "Emerging robotic platforms for minimally invasive surgery," *IEEE Rev. Biomed. Eng.*, vol. 6, pp. 111–126, 2012.

[30] S. Wu, Y. Fan, and Y. Tian, "Sketch of single-incision laparoscopic surgery (sils)," in *Atlas of Single-Incision Laparoscopic Operations in General Surgery*. Springer, 2013, pp. 1–2.

[31] R. Autorino, J. H. Kaouk, J.-U. Stolzenburg, I. S. Gill, A. Mottrie, A. Tewari, and J. A. Cadeddu, "Current status and future directions of robotic single-site surgery: a systematic review," *Eur. Urol.*, vol. 63, no. 2, pp. 266–280, 2013.

[32] Z. Wang, B. Liang, Y. Sun, and T. Zhang, "Adaptive fault-tolerant prescribed-time control for teleoperation systems with position error constraints," *IEEE Trans. Industr. Inform.*, vol. 16, no. 7, pp. 4889–4899, 2020.

[33] Z. Wang, Y. Sun, and B. Liang, "Synchronization control for bilateral teleoperation system with position error constraints: A fixed-time approach," *ISA Transactions*, vol. 93, pp. 125–136, 2019.

[34] Z. Wang, Z. Chen, Y. Zhang, X. Yu, X. Wang, and B. Liang, "Adaptive finite-time control for bilateral teleoperation systems with jittering time delays," *Int. J. Robust Nonlinear Control*, vol. 29, no. 4, pp. 1007–1030, 2019.

[35] S. Rezazadeh, W. Bai, M. Sun, S. Chen, Y. Lin, and Q. Cao, "Robotic spinal surgery system with force feedback for teleoperated drilling," *J. Eng.*, vol. 2019, no. 14, pp. 500–505, 2019.

[36] S. M. Prasad, S. M. Prasad, H. S. Maniar, C. Chu, R. B. Schuessler, and R. J. Damiano Jr, "Surgical robotics: impact of motion scaling on task performance," *J. Am. Coll. Surgeons*, vol. 199, no. 6, pp. 863–868, 2004.

[37] J. Yan and S. E. Salcudean, "Teleoperation controller design using h/sub/spl infin//-optimization with application to motion-scaling," *IEEE Trans. Control Sys. Technol.*, vol. 4, no. 3, pp. 244–258, 1996.

[38] M. Su, H. Wu, S. Gu, J. Huang, Y. Guan, and G. Liu, "Kinematic mapping algorithms for modular master-slave robots," *Robot*, no. 6, p. 11, 2015.

[39] G. A. Holzapfel *et al.*, "Biomechanics of soft tissue," *The handbook of materials behavior models*, vol. 3, pp. 1049–1063, 2001.

[40] T. Hu and J. P. Desai, "Characterization of soft-tissue material properties: large deformation analysis," in *Proc. Int. Symp. Med. Simul.* Springer, 2004, pp. 28–37.

[41] W. Bai, "Research on an intelligent robotic system for single port surgery and its control strategy," Ph.D. dissertation, Shanghai Jiao Tong University, 2019.

[42] J.-P. Merlet, "Jacobian, manipulability, condition number, and accuracy of parallel robots," *ASME J. Mech. Des.*, vol. 128, no. 1, pp. 199–206, 2006.

[43] T. Yoshikawa, "Manipulability of robotic mechanisms," *Int. J. Robot. Res.*, vol. 4, no. 2, pp. 3–9, 1985.

[44] B. Siciliano, L. Sciavicco, L. Villani, and G. Oriolo, *Robotics: modelling, planning and control*. Springer Science & Business Media, 2010.

[45] J. Yao, X. Ding, Q. Zhan, and Q. Zhang, "On task-based directional manipulability of redundant robot," *Robot*, vol. 22, no. 6, 2000.

[46] S. Lee, "Dual redundant arm configuration optimization with task-oriented dual arm manipulability," *IEEE Trans. Robot. Automat.*, vol. 5, no. 1, pp. 78–97, 1989.